

# Tunable Quantum Fluctuation-Controlled Coherent Spin Dynamics

Jun Liang Song and Fei Zhou

*Department of Physics and Astronomy, The University of British Columbia, Vancouver, B. C., Canada V6T1Z1*

(Dated: November 17, 2018)

Temporal evolution of a macroscopic condensate of ultra-cold atoms is usually driven by mean field potentials, either due to scattering between atoms or due to coupling to external fields; and coherent quantum dynamics of this type have been observed in various cold atom experiments. In this article, we report results of studies of a class of quantum spin dynamics which are purely driven by zero point quantum fluctuations of spin collective coordinates. Unlike the usual mean-field coherent dynamics, quantum fluctuation-controlled spin dynamics or *QFCSD* studied here are very sensitive to variation of quantum fluctuations and the corresponding driving potentials induced by zero point motions can be tuned by four to five orders of magnitude using optical lattices. These dynamics have unique dependence on optical lattice potential depths and quadratic Zeeman fields. We also find that thermal fluctuations generally can further enhance the induced potentials although the enhancement in deep optical lattices is much less substantial than in traps or shallow lattices. *QFCSD* can be potentially used to calibrate quantum fluctuations and investigate correlated fluctuations and various universal scaling properties near quantum critical points.

## I. INTRODUCTION

When particles such as atoms interact with each other at low temperatures, very often they exhibit remarkably distinct cooperative behaviors as a result of symmetry breaking. One of the most fascinating and distinct consequences is the possibility of observing quantum dynamics at a macroscopic level [1, 2]. In Bose-Einstein condensates of ultra-cold alkali atoms, macroscopic quantum phenomena related to coherent matter waves[3, 4], AC Josephson effects[5, 6], and vortex lattices[7] have all been observed. Studies of these phenomena in ultra cold matter should eventually lead to applications such as cold-atom-based precise measurements.

Spin correlated macroscopic quantum dynamics have also been a focus of many cold atom experiments carried out recently. Spin ordering and spin-relaxation collisions were first investigated in condensates of sodium atoms by Inouye *et al.* and Miesner *et al.* from Ketterle's group at MIT[8, 9]. Coherent spin dynamics driven by various mean field interactions or external fields were later demonstrated in condensates of hyperfine spin-two rubidium atoms[10], and hyperfine spin-one rubidium atoms[11, 12]. Ordering in spinor gases is usually induced by hyperfine spin dependent two-body scattering[13, 14]. Coherent spin dynamics observed in experiments are related to the coherent quantum dynamics explored in solid state superconductors, and earlier experiments on ultra cold gases of atoms[5, 6]. They are explicit manifestations of fascinating macroscopic quantum states and can be potentially applied towards constructing high precision interferometers. Remarkably, coherent dynamics also provide a unique direct measure of interaction energies or scattering lengths as emphasized before [5, 10, 11].

Quantum fluctuation-controlled spin dynamics or *QFCSD* we are going to study in this article on the other hand are a direct measure of quantum fluctuations; they can be potentially used to calibrate quantum fluctuations and investigate correlated fluctuations near

quantum critical points or universal scaling properties. Furthermore, *QFCSD* of cold atoms can be designed to simulate many other quantum-fluctuation-induced phenomena such as Coleman-Weinberg mechanism of spontaneous symmetry breaking[15], and order due to disorder in antiferromagnets[16, 17]. The system we are examining to understand *QFCSD* is a condensate of rubidium atoms ( $^{87}\text{Rb}$ ) in hyperfine spin-two ( $F = 2$ ) states. The two-body scattering lengths between rubidium atoms have been estimated using both photoassociation data[23, 24, 25, 26], and elastic scattering data near Feshbach resonances[27, 28]. Most recently, Rabi oscillations between different two-spin states have also been used to measure spin dependent interactions[29].

Quantum fluctuations of spin collective coordinates at least have three different effects on spin dynamics. Firstly, quantum fluctuations of wave lengths of condensate sizes usually result in finite-size quantum symmetry restoring. For a spinor condensate of a few million  $^{87}\text{Rb}$  ( $F=2$ ) or  $^{23}\text{Na}$  ( $F=1$ ) atoms, restoring of spin rotational symmetry or quantum diffusion of spin orientation typically occurs at a time scale of a few tens of seconds. So they are not relevant to 10 – 100ms spin dynamics studied in large condensates. The second well-known effect is to renormalize semi-classical spin dynamics, such as spin wave velocities. In high dimensions, dominating contributions are usually from short wave length fluctuations (in optical lattices the shortest wave length is set by lattice constants). These spin fluctuations might also result in quantum phase transitions between spin ordered and disordered states. For most dilute cold atom gases, the renormalization of spin dynamics is perturbative and negligible (except around critical points). And in the limit that interests us, the relative amplitude of spin fluctuations is small. The third effect is to induce dynamics when conventional mean field dynamics are completely frozen out because of degeneracies in a submanifold. This is the limit of *QFCSD* that we are going to study. The dominating contributions in our case

are mainly from quantum fluctuations of an *intermediate* wave length which is comparable to the de Broglie wave length of an atom traveling with spin wave velocities.

However it is quite challenging to probe QFCSD in traps without optical lattices, if not impossible. For dilute gases in the absence of optical lattices, the effective driving potential induced by quantum fluctuations is about  $10^{-5}pk$  per particle (see section III for more discussions) because the relative amplitude of fluctuations is very small. The corresponding dynamics driven by such a small potential are only visible at a time scale of a few thousand seconds, too slow to be observed in current cold atom experiments. In addition, a tiny external magnetic field of strength  $1mG$  can result in a quadratic Zeeman coupling of order of  $6 \times 10^{-3}pk$  for rubidium atoms which is three orders of magnitude larger than the induced potential in dilute gases. In most experiments because of noises in lasers, the effective quadratic Zeeman coupling can be controlled only up to a uncertainty that is equivalent to a magnetic field of an order of  $1mG$ . This further complicates future experimental studies of QFCSD. To resolve these difficulties, we propose to enhance the effect of QFCSD using optical lattices. To vary the amplitude of quantum fluctuations and optimize the effect of fluctuations, we study *QFCSD* in optical lattices where the optical potential depth  $V$  is a convenient tunable parameter[18, 19, 20, 21, 22].

The rest of the article is organized as follows. In section II, we introduce a lattice Hamiltonian to study dynamics of  $^{87}Rb$  atoms in optical lattices and discuss the range of parameters we have used to investigate this phenomenon. In section III, we present our main numerical results on quantum-fluctuation induced potentials, frequencies of coherent dynamics, and how potentials and frequencies depend on optical lattice potential depth. We also study the dynamical stabilities of coherent oscillations when a quadratic Zeeman coupling is present. In section IV, we discuss effects of thermal fluctuations and analyze the potential-depth dependence of thermal enhancement of induced driving potential. In section V, we further investigate effects of spin exchange losses and propose how to observe quantum-fluctuation-controlled spin dynamics within a relatively short life time of  $F = 2$  rubidium atoms. In section VI, we conclude our studies of QFCSD.

## II. MODEL

### A. Microscopic Hamiltonian for spin-two rubidium atoms in optical lattices

In optical lattices, we use the following Hamiltonian that was introduced previously[30, 32],

$$\mathcal{H} = \sum_k \frac{a_L}{2} (\hat{\rho}_k^2 - \hat{\rho}_k) + \frac{b_L}{2} (\hat{\mathcal{F}}_k^2 - 6\hat{\rho}_k) + 5c_L \mathcal{D}_k^\dagger \mathcal{D}_k$$

$$- t_L \sum_{\langle kl \rangle} (\psi_{k,\alpha\beta}^\dagger \psi_{l,\beta\alpha} + h.c.) - \sum_k \mu \hat{\rho}_k + q_B \mathcal{Q}_{zz} \quad (1)$$

Here  $k$  is the lattice site index and  $\langle kl \rangle$  are the nearest neighbor sites,  $\mu$  is the chemical potential and  $t_L$  is the one-particle hopping amplitude,  $q_B$  is the quadratic Zeeman coupling constant.  $a_L$ ,  $b_L$  and  $c_L$  are three interaction constant which have been calculated (see subsection B for more discussions). The single band Hamiltonian is valid when all interaction constants above are much smaller than the energy spacing between centers of two lowest bands.

We have employed the traceless symmetric matrix operator  $\psi^\dagger$  that was introduced previously for the studies of hyperfine spin two rubidium atoms[30]; components  $\psi_{\alpha\beta}^\dagger$ ,  $\alpha, \beta = x, y, z$  are linear superpositions of five spin-2 creation operators,  $\psi_{m_F}^\dagger$ ,  $m_F = 0, \pm 1, \pm 2$  as given above. It is advantageous to use this tensor representation if one is interested in rotational symmetries of condensate wavefunctions, or construction of rotationally invariant operators. We use it to analyze collective spin modes that correspond to small rotations around various axes. The tensor operator  $\psi^\dagger$  is defined in terms of the usual creation operators  $\psi_{m_F}^\dagger$  for five  $F = 2$  states,

$$\begin{aligned} \psi_{\alpha\beta}^\dagger &= \sum_{m_F=0,\pm 1,\pm 2} \mathcal{C}_{\alpha\beta}(m_F) \psi_{m_F}^\dagger; \\ \mathcal{C}_{xz}(\pm 1) &= i\mathcal{C}_{xy}(\mp 2) = \frac{\mp 1}{\sqrt{2}}, \\ \mathcal{C}_{xx}(\pm 2) &= -\mathcal{C}_{yy}(\pm 2) = \frac{\mathcal{C}_{yz}(\pm 1)}{i} = \frac{1}{\sqrt{2}}, \\ \mathcal{C}_{xx}(0) &= \mathcal{C}_{yy}(0) = \frac{\mathcal{C}_{zz}(0)}{-2} = \frac{-1}{\sqrt{3}} \end{aligned} \quad (2)$$

where  $\mathcal{C}_{\alpha\beta}(m_F)$  is symmetric with respect to  $\alpha\beta$ ; all other coefficients are zero. The number operator  $\hat{\rho}$ , the dimer or singlet pair creation operator  $\mathcal{D}^\dagger$ , the total spin operator  $\hat{F}_\alpha$  are defined as  $\hat{\rho} = 1/2 \text{tr} \psi^\dagger \psi$ ,  $\mathcal{D}^\dagger = 1/\sqrt{40} \text{tr} \psi^\dagger \psi^\dagger$ ,  $\hat{F}_\alpha = -i\epsilon_{\alpha\beta\gamma} \psi_{\beta\eta}^\dagger \psi_{\eta\gamma}$ . And the quadratic Zeeman operator  $\mathcal{Q}_{zz}$  is defined as  $\mathcal{Q}_{zz} = \text{tr} \psi^\dagger Q \psi$ , and  $Q_{\alpha\beta} = \delta_{\alpha\beta} \delta_{\beta z}$ .

### B. Range of interaction parameters for the lattice Hamiltonian

Spin correlations between hyperfine spin-two rubidium atoms are determined by three two-body s-wave scattering lengths  $a_F$ ,  $F = 0, 2, 4$ . In optical lattices, local spin-dependent interactions contain two contributions as shown in Eq.(1); one is,  $b_L \mathcal{F}_k^2/2$ , the energy of having total hyperfine spin  $\mathcal{F}_k$  at site  $k$ , and the other is the energy of creating spin singlet pairs (*dimers*),  $5c_L \mathcal{D}_k^\dagger \mathcal{D}_k$  where  $\mathcal{D}_k$  is the dimer creation operator[30]. The usual contact interaction at site  $k$  is of the form  $a_L(\rho_k^2 - \rho_k)/2$ , where  $\rho_k$  is the number of atoms. Three effective coupling constants  $a_L, b_L, c_L$  which characterize various in-

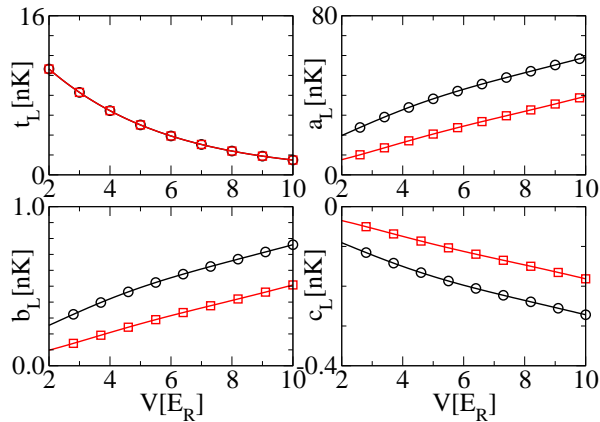


FIG. 1: (Color online) Coupling parameters  $a_L$ ,  $b_L$ ,  $c_L$  and hopping integral  $t_L$  (all in units of  $nk$ ) as a function of optical potential depth  $V$  (in units of recoil energy  $E_R$ ) in 3D (black circles) and 2D (red squares) optical lattices.  $E_R = 3.18kHz$  for  $\lambda = 850nm$  lasers.

teractions are functions of two-body scattering lengths  $a_F$ ,  $F = 0, 2, 4$  and on-site orbitals  $\psi_0(\mathbf{r})$ ,

$$a_L(b_L, c_L) = a(b, c) \frac{4\pi\hbar^2}{m} \int d\mathbf{r} (\psi_0^*(\mathbf{r})\psi_0(\mathbf{r}))^2. \quad (3)$$

Here  $a = (4a_2 + 3a_4)/7$ ,  $b = (a_4 - a_2)/7$  and  $c = (7a_0 - 10a_2 + 3a_4)/35$  are three effective scattering lengths;  $\psi_0$  is the localized Wannier function obtained by solving the Schrodinger equation for an atom in periodical potentials.  $a_L, b_L, c_L$  can then be calculated using the estimates of scattering lengths obtained in Ref.[28]. The range of these parameters for rubidium atoms in optical lattices is plotted in Fig.1.

The range of lattice potential depth is chosen to be from zero up to ten recoil energy or  $10E_R$ . ( $E_R = \hbar^2/2m\lambda^2$ , where  $\lambda$  is the wavelength of lasers.) Below  $2E_R$ , quantum fluctuations turn out to be too weak to induce substantial potential and dynamics. For this reason, we only show numerical results for  $V$  larger than  $2E_R$  but less than  $10E_R$ . Within this range, we find that quantum depletion is usually small, less than twenty percent and our lowest order calculation should suffice. Although quantum fluctuations can be further enhanced above  $10E_R$  and a superfluid-Mott phase transition should take place at  $13E_R$ [18, 19], close to a critical region we however expect a perturbative calculation like the one carried out in this article becomes invalid. The range of atom number density here, or the number of atoms per lattice site  $M$  is from zero to three. Most of data are shown for typical values  $M = 1.0, 2.0, 3.0$ .

For  $F = 2$  rubidium atoms, the quadratic Zeeman coupling  $q_B$  is related to a uniform external magnetic field  $B$  via  $q_B = 3(\mu_B B/2)^2/\Delta$ ,  $\Delta = 6.8GHz$ . Here  $\mu_B$  is the Bohr magneton and  $\Delta$  is the hyperfine splitting. For the

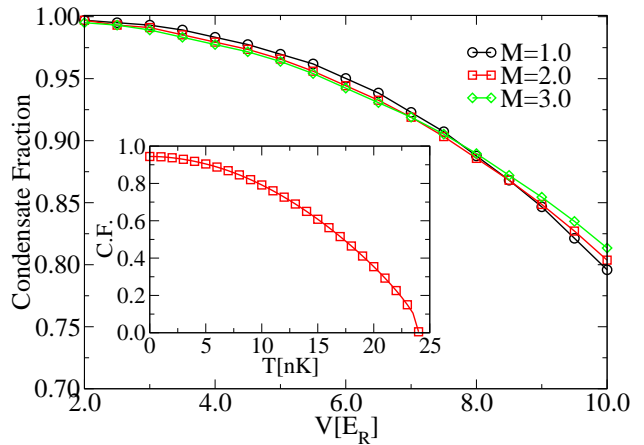


FIG. 2: (Color online) Condensation fraction versus optical lattice potential depth  $V$  (in units of  $E_R$ ). The inset shows the condensate fraction at different temperatures when  $V$  is equal to  $6E_R$ .

purpose of studying *QFCSD*, we set the range of  $B$  to be  $70mG > B > 1mG$  where effects of quantum fluctuations are most visible; beyond  $70mG$  the dynamics are mainly driven by the mean field quadratic coupling  $q_B$  (see section VI for more discussions). The corresponding range for the quadratic Zeeman coupling is then from  $10^{-2}pk$  to  $100pk$ .

### C. Mean field ground states: quantum spin nematics

The coherent spin dynamics of a *uniform* condensate can be described by the evolution of a condensate wavefunction  $\tilde{\chi}$ , i.e. the expectation value of matrix operator  $\psi^\dagger$ . The corresponding equation of  $\tilde{\chi}$  is

$$\begin{aligned} \frac{i}{2} \frac{\partial \tilde{\chi}}{\partial t} &= \frac{\partial H_{sc}}{\partial \tilde{\chi}^*} + \frac{\partial H_Q}{\partial \tilde{\chi}^*} + \frac{\partial H_{qf}}{\partial \tilde{\chi}^*}; \\ \frac{\partial H_{sc}}{\partial \tilde{\chi}^*} &= \frac{a_L}{4} \tilde{\chi} \text{Tr}(\tilde{\chi}^* \tilde{\chi}) + \frac{c_L}{4} \tilde{\chi}^* \text{Tr}(\tilde{\chi} \tilde{\chi}) \\ &\quad + \frac{b_L}{2} [\tilde{\chi}, [\tilde{\chi}^*, \tilde{\chi}]] - (zt_L + \mu/2) \tilde{\chi}, \\ \frac{\partial H_Q}{\partial \tilde{\chi}^*} &= q_B Q \tilde{\chi}. \end{aligned} \quad (4)$$

Here  $H_{sc}$  is the semiclassical Hamiltonian (of matrix  $\tilde{\chi}$ ,  $\tilde{\chi}$ ) obtained previously[30, 31, 32],  $H_Q$  is the quadratic Zeeman coupling term with  $q_B$  being the coupling strength.  $H_{sc}$  and  $H_Q$  (per lattice site) are given by:

$$\begin{aligned} H_{sc} &= \frac{a_L}{8} \text{Tr}(\tilde{\chi}^* \tilde{\chi}) \text{Tr}(\tilde{\chi}^* \tilde{\chi}) + \frac{c_L}{8} \text{Tr}(\tilde{\chi}^* \tilde{\chi}^*) \text{Tr}(\tilde{\chi} \tilde{\chi}) \\ &\quad + \frac{b_L}{4} \text{Tr}[\tilde{\chi}^*, \tilde{\chi}]^2 - (zt_L + \mu/2) \text{Tr}(\tilde{\chi}^* \tilde{\chi}); \end{aligned} \quad (5)$$

$$H_Q = q_B \text{Tr}(\tilde{\chi}^* Q \tilde{\chi}). \quad (6)$$

$z$  is the coordination number of optical lattices. For a field along the  $z$ -direction, matrix  $Q$  is defined as  $Q_{\alpha\beta} = \delta_{\alpha z}\delta_{\beta z}$ . And  $H_{qf}$  is the quantum-fluctuation-induced Hamiltonian discussed below.

For rubidium atoms, scattering lengths estimated in Ref.[24, 25, 26] lead to  $b_L = -10c_L$  while results in Ref.[27, 28] yield  $b_L = -2.8c_L$ . Both calculations show that interaction parameters satisfy  $c_L < 0$  and  $4b_L > c_L$ . As pointed out before[30], in this parameter region without quadratic Zeeman coupling, ground states are spin nematics characterized by real and symmetric tensor wavefunctions  $\tilde{\chi}$  (up to an overall phase). Any condensate that is initially prepared in this submanifold has no mean field dynamics because the potential gradient  $\partial H_{sc}/\partial \tilde{\chi}^*$  vanishes.

To highlight the structure of degenerate ground states, we consider an arbitrary condensate amplitude  $\tilde{\chi}$  in the spin nematic submanifold. It can be parameterized using an  $SO(3)$  rotation,  $\mathcal{R}$  and a  $U(1)$  phase shift  $\phi$ , and a real diagonal traceless matrix  $\chi$ ; i.e.,

$$\begin{aligned} \tilde{\chi}(X_x, X_y, X_z, \xi, \phi) &= \sqrt{4M} e^{i\phi} \mathcal{R}^T \chi(\xi) \mathcal{R}, \\ \mathcal{R}(X_x, X_y, X_z) &= \exp(T^x X_x + T^y X_y + T^z X_z) \end{aligned} \quad (7)$$

where  $M$  is the number density or average number of atoms per lattice site.  $\mathcal{R}$  is an  $SO(3)$  rotation matrix defined by three spin angles  $X_\alpha$ ,  $\alpha = x, y, z$ , and anti-symmetric generators  $T_{\beta\gamma}^\alpha = -\epsilon_{\alpha\beta\gamma}$ .  $\chi(\xi)$ ,  $\xi \in [0, 2\pi]$ , are normalized real diagonal traceless matrices that form a family of solutions specified by a single parameter  $\xi$ [32];

$$\chi_{\alpha\alpha} = \frac{\sin(\xi - \xi_\alpha)}{\sqrt{3}}, \quad (8)$$

and  $\xi_x = \pi/6$ ,  $\xi_y = 5\pi/6$  and  $\xi_z = 3\pi/2$ . Nematics with different  $\xi$  exhibit different spin configurations. Following the definition of tensor operator in Eq.(2), one can easily show that these solutions represent condensates of spin-two atoms specified by five-component wavefunctions  $\psi^T = (\psi_2, \psi_1, \psi_0, \psi_{-1}, \psi_{-2})$  and

$$\psi^T = \sqrt{M} \left( \frac{\sin \xi}{\sqrt{2}}, 0, \cos \xi, 0, \frac{\sin \xi}{\sqrt{2}} \right). \quad (9)$$

So in a more conventional representation, these states labeled by value  $\xi$  correspond to condensates where all atoms occupy a particular spin-2 state,

$$|\xi \rangle = \cos \xi |2, 0 \rangle + \frac{\sin \xi}{\sqrt{2}} (|2, 2 \rangle + |2, -2 \rangle). \quad (10)$$

It is worth pointing out that spin nematics here are time-invariant; the expectation value of the hyperfine spin operator  $\mathcal{F}_k$  in these states is zero. However, all nematics have the following nonzero quadrupole spin order (up to an  $SO(3)$  rotation),

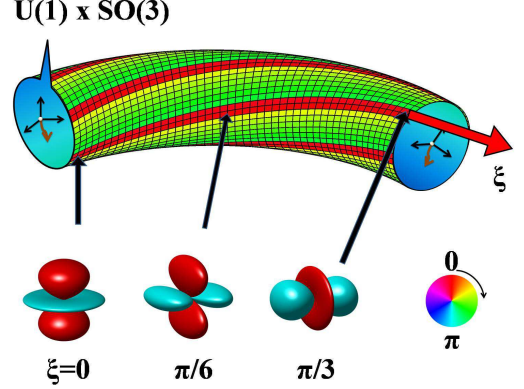


FIG. 3: (Color online) An artistic view of the five-dimension manifold of spin nematics. Three  $SO(3)$  rotation degrees and  $U(1)$ -phase degree are represented by a cross section at a given spin deformation angle  $\xi$ . We have also plotted the nematic wavefunctions  $\psi_S(\theta, \phi) = \sum_{\alpha\beta} \chi_{\alpha\beta} n_\alpha n_\beta$  as a function  $\theta, \phi$  in a spherical coordinate.  $n_\alpha$ , is the  $\alpha$ th component of a unit vector  $\mathbf{n}(\theta, \phi)$  and colors indicate phases of wavefunctions.

$$\begin{aligned} \mathcal{O}_{\alpha\beta} &= \langle \mathcal{F}_{k\alpha} \mathcal{F}_{k\beta} \rangle - \frac{1}{3} \delta_{\alpha\beta} \langle \mathcal{F}_k^2 \rangle, \\ \mathcal{O}_{\alpha\beta} &= 2M \sin(2\xi + \xi_\alpha) \delta_{\alpha\beta}. \end{aligned} \quad (11)$$

Therefore, the nematic submanifold is effectively a five-dimension space that is characterized by five collective coordinates  $X_\nu$ ,  $\nu = x, y, z, \xi, p$ : three spin rotational angles  $X_\alpha$  ( $\alpha = x, y, z$ ), one spin deformation  $\xi$ -angle  $X_\xi$  (or  $\xi$ ) specifying spin configurations and one phase angle  $X_p (= \phi)$ . Furthermore, it is easy to verify that up to an  $SO(3)$  rotation and a phase factor, states at  $\xi$  and at  $\xi + \pi/3$  are equivalent and the fundamental period of this characterization is  $\pi/3$ . When the system is rotationally invariant (i.e. no external fields), we also find that  $E(\xi) = E(\xi + \pi/3)$  and  $E(\xi) = E(-\xi)$ .  $E(\xi)$  is the energy of a state defined by  $\xi$ .

#### D. Effective Hamiltonian for QFCSD

To investigate the kinetic energy and quantum fluctuation-induced potential energy for dynamics of a condensate initially prepared in this submanifold, we expand tensor  $\psi_{\alpha\beta}^\dagger$  about a reference condensate wavefunction  $\chi(\xi)$  in terms of five collective coordinates  $X_\nu$  introduced above and their conjugate operators  $\hat{P}_\nu$ . We furthermore separate the macroscopic dynamics of condensates ( $\mathbf{q} = 0$ -mode) from the microscopic zero point quantum fluctuations ( $\mathbf{q} \neq 0$  mode). And we restrict ourselves to the dynamics of a condensate in a linear regime.

In the *appendix*, using the decomposition introduced in Eq.(A1) we expand the Hamiltonian in Eq.(1) in terms of collective coordinates  $X_\nu$ ,  $\hat{P}_\nu$  and obtain an effective Hamiltonian for submanifold dynamics. Up to the quadratic order, the Hamiltonian contains two sectors, one involving operators of  $\mathbf{q} = 0$ -mode and the other one only involving operators of  $\mathbf{q} \neq 0$ . The Hamiltonian for the  $\mathbf{q} = 0$  sector generates the kinetic energy needed for the dynamics along five orthogonal directions. The corresponding effective masses can be expressed in terms of scattering lengths  $a_{0,2,4}$ , and quadratic Zeeman coupling  $q_B$ . In addition, the expansion of the quadratic Zeeman term  $H_Q$  for  $\mathbf{q} = 0$  mode also generates a mean field potential  $V_Q$ . This potential  $V_Q$  as illustrated below always favors a biaxial nematic with  $\xi = \pi/2$ . The biaxial nematic has dihedral-four ( $Dih_4$ ) symmetries with easy axes in the  $xy$ -plane[32]. On the other hand, the sector of Hamiltonian for  $\mathbf{q} \neq 0$  collective modes contains zero point energies of those modes. These energies in general depend on spin configurations or the values of  $\xi$ . So quantum fluctuations of collective coordinates effectively induce a  $\xi$ -dependent potential  $V_{qf}$  in the submanifold; this potential alone selects out a unique ground state as recently pointed out by Song *et al* [32] and Turner *et al* [33]. For rubidium atoms with a positive  $b_L$ , previous calculations show that the ground state is a uniaxial nematic in the absence of quadratic Zeeman coupling. Turner *et al* also pointed out that thermal fluctuations further enhance the amplitude of induced potentials and this order-from-disorder phenomenon is robust against finite temperatures[33].

We now study the dynamical consequences of both quadratic Zeeman coupling  $H_Q$  and zero point quantum fluctuations  $H_{qf}$ . For simplicity, we are mainly focused on dynamics around

a) a *uniaxial nematic* at  $\xi = 0$  or a condensate with rubidium atoms occupying hyperfine spin state  $|2, 0 \rangle$ ;

b) a *biaxial nematic* at  $\xi = \pi/2$  or a condensate with rubidium atoms occupying hyperfine spin state  $(|2, 2 \rangle + |2, -2 \rangle)/\sqrt{2}$ .

The resultant Hamiltonian for oscillations around a state  $\xi$  ( $\xi = 0$  or  $\pi/2$ ) can be cast in the following form,

$$H_{qf} = \sum_{\nu} \frac{\hat{P}_{\nu}^2}{2N_T m_{\nu}} + N_T (V_{qf}(\xi, X_{\xi}) + V_Q(\xi, X_{\nu})),$$

$$V_{qf}(\xi, X_{\xi}) = \frac{1}{2N_T} \sum_{\mathbf{q} \neq 0} \sum_{\nu} E_{\nu, \mathbf{q}}(\xi, X_{\xi}, q_B),$$

$$V_Q(\xi, X_{\nu}) = \frac{4Mq_B}{3} \cos^2(\xi + X_{\xi}) + 4Mq_B \sum_{\alpha} \kappa_{\alpha} X_{\alpha}^2. \quad (12)$$

In Eq.(12),  $N_T$  is the number of lattice sites and  $M$  is the average number of atoms per site. The masses for five directions are calculated to be

$$m_p = \frac{1}{a_L + c_L}, m_{\xi} = \frac{2M}{q_B \kappa_{\xi} - 2Mc_L},$$

$$m_{\alpha} = \frac{8MG_{\alpha\alpha}}{8Mb_L G_{\alpha\alpha} - 2Mc_L + \kappa_{\alpha} q_B G_{\alpha\alpha}^{-1}}. \quad (13)$$

$\kappa_{x,y,z,\xi}$  are  $\xi$ -dependent;  $\kappa_{x(y)} = \chi_{xx(yy)}^2 - \chi_{zz}^2$ ,  $\kappa_z = 0$  and is independent of  $\xi$ ;  $\kappa_{\xi} = 4(\chi_{zz}^2 - \chi_{zz}^2)$  is a function of  $\xi$  and is  $-4/3$  when  $\xi = 0$ , and  $4/3$  when  $\xi = \pi/2$ ;  $\dot{\chi}_{zz} = d\chi_{zz}/d\xi$ .  $G_{\alpha\alpha}(\xi)$ ,  $\alpha = x, y, z$  is a function of  $\xi$ ,  $G_{xx,yy}(\xi) = \sin^2(\xi \mp \frac{2\pi}{3})$ ,  $G_{zz} = \sin^2 \xi$ .  $E_{\nu, \mathbf{q}}(\xi, X_{\xi}, q_B)$  is the energy of a mode- $\nu$  ( $\nu = x, y, z, \xi, p$ ) collective excitation with crystal momentum  $\mathbf{q}$ , and is a function of parameters  $\xi$ ,  $X_{\xi}$ , and quadratic Zeeman coupling  $q_B$ . In the *appendix*, we show the general form of this energy explicitly for the case of nonzero  $q_B$ . Only spin modes with  $\nu = x, y, z, \xi$  contribute to the  $\xi$ -dependence of potential  $V_{qf}$ . Fluctuations of phase modes are independent of parameter  $\xi$  or Zeeman coupling  $q_B$  and are irrelevant for discussions of spin dynamics as a result of spin-phase separation. Note that  $V_{qf}$  is a function of  $\xi$ ,  $q_B$  and  $X_{\xi}$ ; and  $V_Q$  is a function of  $\xi$ ,  $q_B$  and  $X_{\nu}$ ,  $\nu = x, y, z, \xi$ .

### III. MAIN RESULTS FOR QFCSD

#### A. Potentials induced by quantum fluctuations

We first consider a situation where the quadratic Zeeman coupling is absent and the potential  $V_Q$  vanishes. As argued before, generally speaking  $V_{qf}(\xi, 0) = V_{qf}(\xi + \pi/3, 0)$  and  $V_{qf}(\xi, 0) = V_{qf}(-\xi, 0)$ . The explicit form of  $V_{qf}$  calculated here indeed is consistent with this general requirement. We also find that the main contribution to  $V_{qf}$  is from fluctuations of wavelength  $1/(m_{BN}v_{\alpha})$  that is much longer than the lattice distance  $d_L$ . More specifically, following discussions in the *appendix*, the  $\xi$ -dependent induced potential can be written as a sum of polynomials of spin-wave velocities, i.e.  $\sum_{\alpha} v_{\alpha}^{d+2}$  for  $d$ -dimension optical lattices. Spin-wave velocities are functions of  $c_L, b_L$  and  $t_L$ . We numerically integrate over all wavelengths and obtain the  $\xi$ -dependence of  $V_{qf}$  as shown in the inset of Fig.4.

Consequently, we find that in  $d$ -dimension lattices ( $d = 2, 3$ ), the barrier height  $B_{qf}$  which is defined as  $V_{qf}(\frac{\pi}{6}, 0) - V_{qf}(0, 0)$ , the energy difference between  $\xi = \pi/6$  and  $\xi = 0$  satisfies the following simple scaling function,

$$B_{qf} = \frac{|Mc_L|^{\frac{d+2}{2}}}{t_L^{\frac{d}{2}}} g_d\left(\frac{b_L}{c_L}, \frac{M|c_L|}{t_L}\right). \quad (14)$$

Here  $g_d(x, y)$  is a dimensionless function that can be studied numerically. This scaling function is either insensitive to the variation of  $y$  as for  $d = 3$  [32] or independent of  $y$  as for  $d = 2$ .

We also study the barrier height  $B_{qf}$  as a function of  $V$ , the potential depth of optical lattices. We find that in the absence of lattice potentials or in traps, for a density that is equivalent to one particle ( $M = 1.0$ ) per lattice

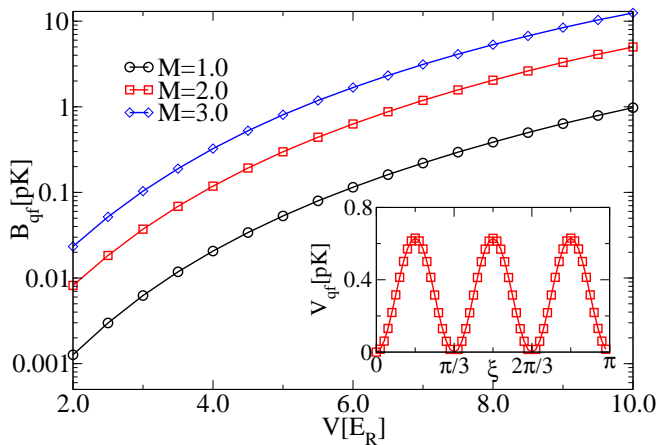


FIG. 4: (Color online) Barrier height  $B_{qf}$  (in units of pK) as a function of optical potential depth  $V$  (in units of recoil energy  $E_R$ ). Inset is for the  $\xi$ -dependence of  $V_{qf}$ , a potential induced by quantum fluctuations when  $V = 6E_R$  and  $M = 2.0$ .

site the barrier height is of order of  $10^{-5}$  to  $10^{-4}pk$  and is negligible in experiments. When the optical lattice potential depth  $V$  is varied, the barrier height typically increases by four or five orders of magnitude. Particularly, as  $V$  increases from  $2E_R$  to  $10E_R$ , mean field interaction energies  $a_L, b_L, c_L$  vary by less than a factor of three; however, for the same range of  $V$ , the barrier height  $B_{qf}$  varies from  $10^{-3}pk$  to a few  $pk$ . The energy shift between the uniaxial state at  $\xi = 0$  and biaxial state at  $\xi = \pi/6$  is analogous to the Lamb shift observed in atoms[34]. In Fig.4, we show the barrier height  $B_{qf}$  of induced potential versus lattice potential depth  $V$ .

In Fig. 5, we further plot the effective potential  $V_{eff} = V_Q + V_{qf}$  as a function of optical potential depth  $V$ . When  $V$  is less than  $V_c$ , the biaxial nematic with  $\xi = \pi/2$  is stable and as  $V > V_c$ , it becomes locally unstable. For  $^{87}Rb$  atoms with one atom per lattice site ( $M = 1.0$ ),  $V_c$  is about  $5.5E_R$  ( $E_R$  is the recoil energy of optical lattices) when the quadratic Zeeman coupling is  $10pk$ . Almost opposite behaviors are found for uniaxial nematics at  $\xi = 0$ . Values of  $\xi$  at which global potential minima are found are shown as a function of  $V_{eff}$  in Fig. 5b.

## B. Oscillations induced by quantum fluctuations

To understand the dynamical consequences of  $V_{qf}$ , we consider coherent dynamics around the uniaxial nematic state at  $\xi = 0$  that is selected out by the fluctuation-induced potential  $V_{qf}$  or the biaxial nematic state at  $\xi = \pi/2$  that is favored by the quadratic Zeeman potential  $V_Q$ . Particularly we are interested in oscillations along the  $X_\xi$ -direction around state  $\xi = 0$  or  $\pi/2$ . These motions correspond to the following time evolution of condensates,

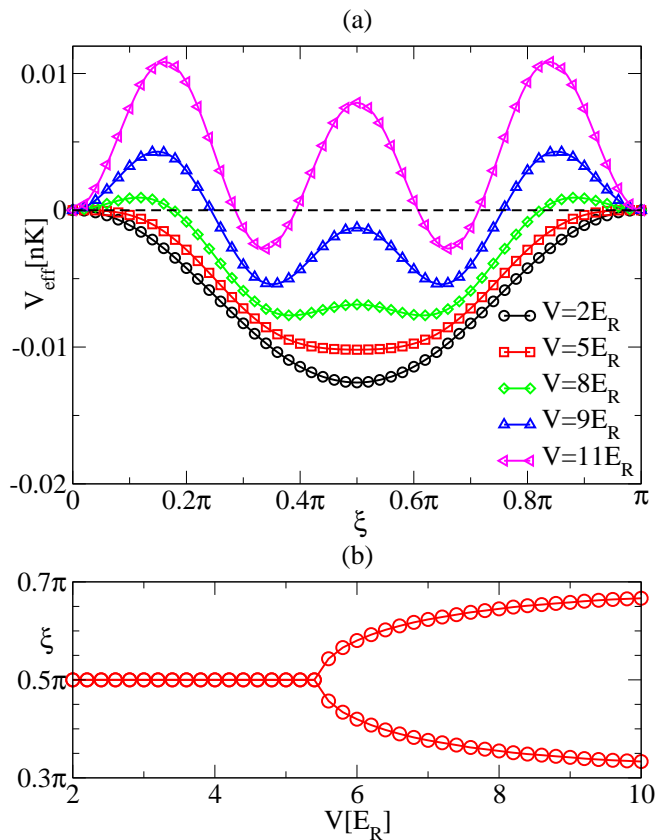


FIG. 5: (Color online) (a) Effective potential  $V_{eff} = V_Q + V_{qf}$  (in units of  $nk$ ) as a function of  $\xi$  for various optical potential depth  $V$  (in units of recoil energy  $E_R$ ) of 3D lattices. The quadratic Zeeman coupling strength is set to be  $10pk(31mG)$  and number of atoms per lattice site  $M$  is equal to one. (b) Values of  $\xi$  at which global potential minima in (a) are found are plotted as a function of optical potential depth  $V$ .

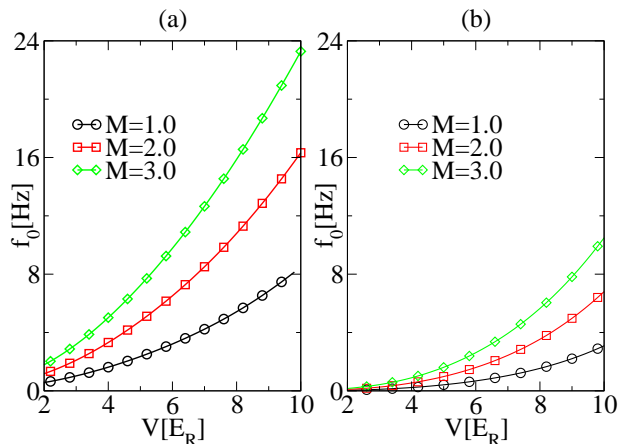


FIG. 6: (Color online) (a),(b), frequencies  $f_0 = \Omega_0 / (2\pi)$  for population oscillations around  $|2, 0\rangle$  state are shown as a function of potential depth  $V$  in (a) 2D and (b) 3D optical lattices for different atom number density  $M$ ; here the quadratic Zeeman coupling is absent.

$$\begin{aligned}
|t\rangle &\approx (\cos \xi - \sin \xi X_0 F(t)) |2, 0\rangle + \\
&\frac{1}{\sqrt{2}} (\sin \xi + \cos \xi X_0 F(t)) (|2, 2\rangle + |2, -2\rangle); \\
F(t) &= \cos \frac{\Omega}{2} t + i \frac{m_\xi \Omega}{4M} \sin \frac{\Omega}{2} t
\end{aligned} \tag{15}$$

where  $X_0$  is the initial deviation from state  $\xi = 0$  or  $\pi/2$  and  $m_\xi$  is the effective mass given in Eq.(13). By solving the equation of motion in Eq.(12) including the quadratic Zeeman effects, we derive a general expression for oscillation frequencies  $\Omega(q_B, V)$  in general is a function of the quadratic Zeeman coupling  $q_B$ , optical lattice potential depth  $V$ , and the number density  $M$ . For population oscillations around  $\xi = 0$  or  $\pi/2$ , we obtain the following frequencies

$$\Omega = 2\sqrt{\left(\sigma \frac{8Mq_B}{3} + V''_{qf}\right) \left(\sigma \frac{2q_B}{3M} + |c_L|\right)}; \tag{16}$$

here  $\sigma = \mp 1$  for  $\xi = 0$  and  $\pi/2$  respectively.  $V''_{qf}$  is the curvature of potentials at  $\xi = 0$  or  $\pi/2$ .

Note that both the real and imaginary part of  $F(t)$  oscillate as a function of time; thus unless  $\frac{m_\xi \Omega}{4M}$  is exactly equal to one which only occurs when atoms are noninteracting or the quadratic Zeeman coupling  $q_B$  is infinite, the magnitude of  $F(t)$  oscillates as the time varies. Practically, in most cases we examine below,  $m_\xi \Omega$  turns out to be much less than unity because both the curvature  $V''_{qf}$  and the Zeeman coupling  $q_B$  are smaller than the inverse of effective mass  $m_\xi$ , or the spin interaction energy  $c_L$ ; thus oscillations of the imaginary part of  $F(t)$  can be neglected. Oscillations along the direction of  $X_\xi$  therefore always lead to temporal oscillations in population of rubidium atoms in either  $|2, 0\rangle$  or  $|2, \pm 2\rangle$  states that can be observed in experiments.

We first examine the cases when the quadratic Zeeman coupling is absent i.e.  $q_B = 0$ . The frequency in this limit is a direct measure of quantum fluctuations and  $\Omega_0 = \Omega(q_B = 0, V) = 2\sqrt{V''_{qf}|c_L|}$ . In the absence of lattice potentials, or in traps we find that oscillation frequencies are about  $10^{-3}$ Hz. At finite temperatures, thermal fluctuations do enhance oscillation frequencies by a factor of two to four; however, this is far from sufficient for the experimental study of *QFCS*D within the life time of these isotopes[10].

In optical lattices, we find that the enhancement of spin-dependent interactions  $b_L, c_L$ , and especially the rapid increasing of band mass  $m_{BN}$  can result in oscillation frequencies of order of a few Hz, which are about three to four orders of magnitude higher than those in traps. The scaling behavior of  $\Omega_0$  is closely related to that of  $B_{qf}$ . Taking into account the expression for effective mass  $m_\xi$ , we find

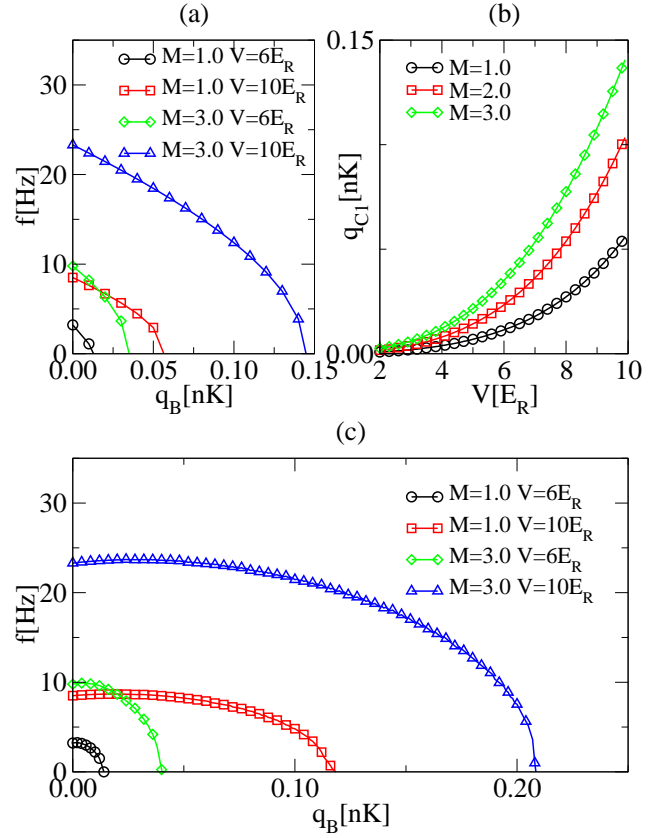


FIG. 7: (Color online) Frequencies  $f = \Omega/(2\pi)$  for population oscillations as a function of quadratic Zeeman coupling  $q_B$  (in units of  $nk$ ) for various potential depth  $V$  in 2D optical lattices with  $M$  atoms per lattice site. (a) for oscillations along the  $X_\xi$ -direction around state  $|2, 0\rangle$ ; dynamics are unstable above a threshold  $q_{c1}(V)$ . The  $V$ -dependence of  $q_{c1}$  (in units of  $nk$ ) is shown in (b). (c) is for oscillations around states with  $\xi = \xi_m (< \pi/2)$  at which global potential minima shown in Fig.5(a) are found. (see also Eq.(15))

$$\Omega_0 \sim \frac{M^{\frac{d+2}{4}} |c_L|^{\frac{d+4}{4}}}{t_L^{\frac{d}{4}}} g_d^{\frac{1}{2}} \left( \frac{b_L}{c_L}, \frac{M|c_L|}{t_L} \right). \tag{17}$$

In Fig. 6, we show the plot of  $f_0 = \Omega_0/2\pi$ , the oscillation frequency versus  $V$  in the absence of Zeeman coupling  $q_B$ .

Experimental studies of *QFCS*D can also be carried out by investigating dynamics of rubidium atoms in the presence of finite quadratic Zeeman coupling  $q_B$ . The submanifold dynamics now are driven by both quadratic Zeeman coupling and quantum fluctuations. There are three main modifications to the effective Hamiltonian  $H_{eff}$ . Firstly, according to Eq.(13), effective masses now depend on the quadratic Zeeman coupling  $q_B$ . Secondly, following discussions in the *appendix*, among four spin collective modes ( $\nu = x, y, z, \xi$ ) and one phase mode ( $\nu = p$ ), two of spin modes,  $x$ - and  $y$ -mode, can be gapped and one,  $z$ -mode, always remains gapless. Details of spec-

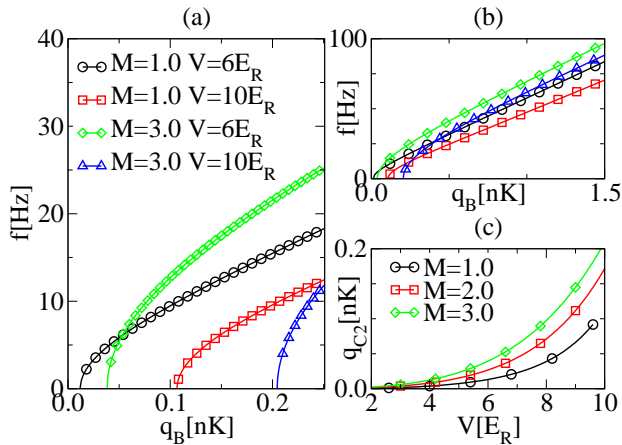


FIG. 8: (Color online) (a), (b) Frequencies  $f = \Omega/(2\pi)$  for oscillations along the  $X_\xi$ - direction around biaxial nematic state  $|2, 2 \rangle + |2, -2 \rangle$  versus quadratic Zeeman coupling  $q_B$  (in units of  $nk$ ) for various optical potential depth  $V$  in 2D optical lattices with  $M$  atoms per lattice site. (a) is for population oscillations close to the threshold  $q_{c2}$  and (b) is for away from  $q_{c2}$ . Oscillations are unstable below a threshold  $q_{c2}$ ; in (c),  $q_{c2}$  (in units of  $nk$ ) as a function of  $V$  is shown.

tra of  $\xi$ -mode depend on the value of  $\xi$ ; excitations are unstable when  $\kappa_\xi$  is negative and are gapped when  $\kappa_\xi$  are positive. The energy gap of stable  $\xi$ -mode excitations depends on  $\xi$  and becomes maximal at  $\xi = \pi/2$ . Finally, a mean field quadratic Zeeman potential that depends on  $X_\xi$  and  $X_\alpha$ ,  $\alpha = x, y, z$ , is also present and modifies the spin dynamics. Oscillation frequencies  $\Omega$  as a function of quadratic Zeeman coupling  $q_B$  for various potential depth  $V$  can be calculated explicitly using Eq.(16). Plots of these results are shown in Fig.7,8.

In the limit of weak quadratic Zeeman coupling,  $QFCS$ D can be most conveniently studied around the uniaxial nematic state at  $\xi = 0$ , or  $|2, 0 \rangle$  state[35]. For rubidium atoms, this is the ground state when the quadratic Zeeman coupling is absent, and remains to be locally stable along the direction of  $X_\xi$  up to a finite  $q_{c1}$ . When the quadratic Zeeman coupling  $q_B$  is much smaller than  $q_{c1}$ , the effective potential  $V_{eff}$  is mainly due to the quantum-fluctuation induced one,  $V_{qf}$ . Above  $q_{c1}$ , a dynamical instability occurs and a perturbation along the  $X_\xi$ -direction around  $|2, 0 \rangle$  starts to grow exponentially. We find that in traps where  $V = 0$ ,  $q_{c1}$  is about  $10^{-2}pk$ ; in optical lattices when  $V$  varies between  $2E_R$  to  $10E_R$ , the value of  $q_{c1}$  increases from  $0.1pk$  up to about  $0.1nk$ . And as  $q_B$  approaches zero, the oscillation frequency  $\Omega(q_B, V)$  saturates at the value  $\Omega_0$  shown in Fig.6. The  $q_B$ -dependence of frequencies for oscillations around  $\xi = 0$  is shown in Fig.7; near  $q_B = q_{c1}$ , the frequencies scale as  $\sqrt{q_{c1} - q_B}$ . Alternatively, one can also study oscillations around states at which global potential minima of  $V_{eff}$  are found; similar  $q_B$ -dependence is shown in Fig.7c.

At relatively high frequencies, convenient oscillations

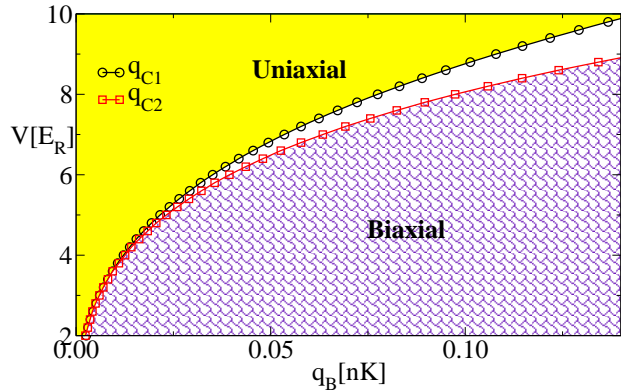


FIG. 9: (Color online) Regions of dynamical stability in the  $V - q_B$  plane for three particles per lattice site ( $M = 3.0$ ). Oscillations around uniaxial nematic or state  $|2, 0 \rangle$  (biaxial nematic or state  $|2, 2 \rangle + |2, -2 \rangle$ ) are locally stable along the  $X_\xi$ -direction in the yellow shaded (purple patterned) area; dynamical instabilities occur when  $q_B > q_{c1}(V)$  ( $q_B < q_{c2}(V)$ ).  $q_B$  is in units of  $nk$ .

to investigate are the ones along the  $X_\xi$  direction around the biaxial nematic state at  $\xi = \pi/2$  point or  $(|2, 2 \rangle + |2, -2 \rangle)/\sqrt{2}$  state. This state becomes stable when  $q_B$  is larger than  $q_{c2}$  and oscillations are well defined only in this limit. When  $q_B$  is smaller than this critical value, the dynamics are mainly driven by quantum fluctuations and oscillations are unstable. In the vicinity of  $q_{c2}$ , the oscillation frequency again scales as  $\sqrt{q_B - q_{c2}}$ . When  $q_B$  is much bigger than  $q_{c2}$  but smaller than  $c_L$ , the frequency is proportional to  $\sqrt{q_B}$ ; in this limit, the potential  $V_{eff}$  is already dominated by the quadratic Zeeman term, or  $V_Q$ , but the effective mass is mainly induced by spin dependent interactions.

When the quadratic Zeeman coupling further increases well above the value of  $c_L$ , relatively fast dynamics are now mainly driven by the external coupling and the frequency  $\Omega$  approaches  $8q_B/3$ , which is equal to the quadratic Zeeman splitting between state  $|2, 0 \rangle$  and  $|2, \pm 2 \rangle$ . In this limit, scattering between atoms during a short period of  $2\pi/\Omega$  becomes negligible; the population oscillations due to scattering or interactions are therefore significantly suppressed as here hyperfine spin two atoms are effectively *noninteracting*. Indeed, following the expression for  $F(t)$  in Eq.(15) and Eq.(13),(16), one finds that the amplitude of population oscillations scales as  $1/q_B$  at large  $q_B$  limit and  $F(t)$  becomes  $\exp(i4q_B t/3)$  when  $q_B$  approaches infinite, i.e., a pure phase factor with a constant modulus.

In Fig.8, we show that the  $q_B$ -dependence of oscillation frequencies both close to the threshold  $q_{c2}$  and away from  $q_{c2}$ . As we have mentioned before,  $QFCS$ D is rather sensitive to the variation in  $V$ .  $q_{c1}$  and  $q_{c2}$  as functions of  $V$  are shown in Fig. 7,8.

So far we have studied coherent dynamics driven by potentials induced by quantum fluctuations at zero tem-



perature. In the following section, we analyze the effect of temperatures, or thermal fluctuations.

#### IV. EFFECTS OF THERMAL FLUCTUATIONS

We now turn to the effect of temperatures and focus on three-dimensional optical lattices. At a finite temperature, collective modes including spin waves are thermally excited. The occupation number of  $\alpha$ th spin-wave excitations with momentum  $\hbar q$  and energy  $E_{\alpha,q}$  is

$$n(\alpha, q) = \frac{1}{e^{\frac{E_{\alpha,q}}{kT}} - 1}. \quad (18)$$

The free energy density (or per lattice site) of a condensate characterized by  $\xi$  is

$$F(\xi, T, V) = \frac{1}{N_T} \sum_{\alpha, q} \left( \frac{E_{\alpha,q}}{2} + kT \ln(1 - e^{-\frac{E_{\alpha,q}}{kT}}) \right). \quad (19)$$

Just as in the zero temperature case because of the  $\xi$ -dependence of spin wave velocities, the free energy density also depends on the values of  $\xi$  and the main contribution to the  $\xi$ -dependence of free energy density is again from fluctuations of wavelength  $1/(m_{BN}v_\alpha)$ , or of a characteristic energy  $T_*$  that is of an order of  $|c_L|$  (or  $b_L$ ). Thermal fluctuations become more important than quantum ones when temperatures are much higher than  $T_*$ . The other temperature effect is from the temperature dependence of spin wave velocities  $v_\alpha$ . Because of the thermal depletion, spin wave velocities  $v_\alpha$  ( $\alpha = x, y, z$ ) decrease as temperatures increase and become zero when the BEC temperature  $T_{BEC}$  is approached. Therefore the temperature dependence of free energy are determined by two dimensionless quantities,  $T/T_*$  and  $T/T_{BEC}$ . In all cases we are going to study below,  $T_*$  (of order of  $-c_L$ ) is less or much less than  $T_{BEC}$ .

We study the asymptotics of free energy in low temperature ( $T \ll T_*$ ) and high temperature ( $T \gg T_*$ ) limits. When  $T \ll T_*$ , only modes with energy much smaller than  $T_*$  are thermally occupied. Therefore contributions from these thermal excitations can be calculated by substituting quasi-particle spectra  $E_{\alpha,q}$  approximately with phonon-like spectra  $v_\alpha q$ . One then obtains the following expression for the free energy per lattice site (up to a constant)

$$F(\xi, T, V) = V_{qf} \left( 1 - \left( \frac{T}{T_{BEC}} \right)^{\frac{3}{2}} \right)^{\frac{5}{2}} - \frac{\pi^2 kT}{90} \sum_{\alpha} \left( \frac{d_L kT}{v_\alpha} \right)^3. \quad (20)$$

The barrier height,  $B_{th}(T, V) = F(\xi = \frac{\pi}{6}, T, V) - F(\xi = 0, T, V)$ , can be calculated accordingly and the asymptotics at low temperatures is

$$B_{th}(T, V) - B_{th}(0, V) \sim \frac{|c_L|^{5/2}}{t_L^{3/2}} \left( \frac{kT}{|c_L|} \right)^4. \quad (21)$$

Here we have neglected the term depending on  $T/T_{BEC}$  because we are interested in temperatures much less than  $T_{BEC}$ . (Such a term is only important at very low temperatures that are of an order of  $|c_L|(|c_L|/T_{BEC})^{3/5} (\ll T_*)$ ). Therefore, the low temperature enhancement of  $B_{th}$  is mainly from the "black-body" radiation of spin wave excitations.

When  $T \gg T_*$ , spin modes with energy much bigger than  $T_*$  are thermally occupied. For modes of energy  $T_*$ , we can approximate  $n(\alpha, q)$  with a classical result  $n(\alpha, q) = kT/E_{\alpha,q}$ . Our scaling analysis of the free energy per lattice site shows that in this limit,

$$F(\xi, T, V) = -\frac{2kT}{3\pi} \sum_{\alpha} \left( \frac{v_\alpha}{4d_L t_L} \right)^3 \left( 1 - \left( \frac{T}{T_{BEC}} \right)^{\frac{3}{2}} \right)^{\frac{3}{2}}. \quad (22)$$

The barrier height,  $B_{th}(T, V) = F(\xi = \frac{\pi}{6}, T, V) - F(\xi = 0, T, V)$ , can be calculated accordingly and asymptotics at high temperatures are

$$B_{th}(T, V) \sim \frac{c_L^{5/2}}{t_L^{3/2}} \frac{kT}{c_L} \left( 1 - \left( \frac{T}{T_{BEC}} \right)^{\frac{3}{2}} \right)^{\frac{3}{2}}. \quad (23)$$

The above result shows that at relatively high temperatures thermal spin wave fluctuations enhance induced potentials and this enhancement is characterized by a linear function of  $kT/|c_L|$  or  $kT/T_*$ . However, because of the thermal depletion of condensates at finite temperatures, there is an overall suppression given by a factor  $1 - (T/T_{BEC})^{3/2}$ . The competition between these two effects results in a maxima in the free energy density. That is at temperatures larger than  $T_*$  but much smaller than  $T_{BEC}$ , the free energy increases linearly as a function of temperature until the thermal depletion becomes significant. The maximal enhancement is therefore about  $T_{BEC}/T_*$ . At further higher temperatures, the free energy density decreases and near  $T_{BEC}$ , its temperature dependence is mainly determined by a factor  $(1 - (T/T_{BEC})^{3/2})^{3/2}$  as shown in Eq.(23).

Evidently, the magnitude of maximal enhancement is very much dependent on the ratio between  $T_{BEC}$  and  $T_*$ . In optical lattices, the magnitude of BEC transition temperatures for averagely one or two particles per lattice is mainly set by the band width  $t_L$  while  $T_*$  is determined by  $|c_L|$ . This ratio therefore the enhancement is quite sensitive to the optical lattice potential depth  $V$ . We find that the enhancement in the absence of lattice potentials is substantial and thermal fluctuations increase the induced potential by about a factor of fifty. This is consistent with a previous calculation[33]. However, when the lattice potential depth increases,  $c_L$  increases but  $t_L$  decreases, the thermal enhancement becomes much less

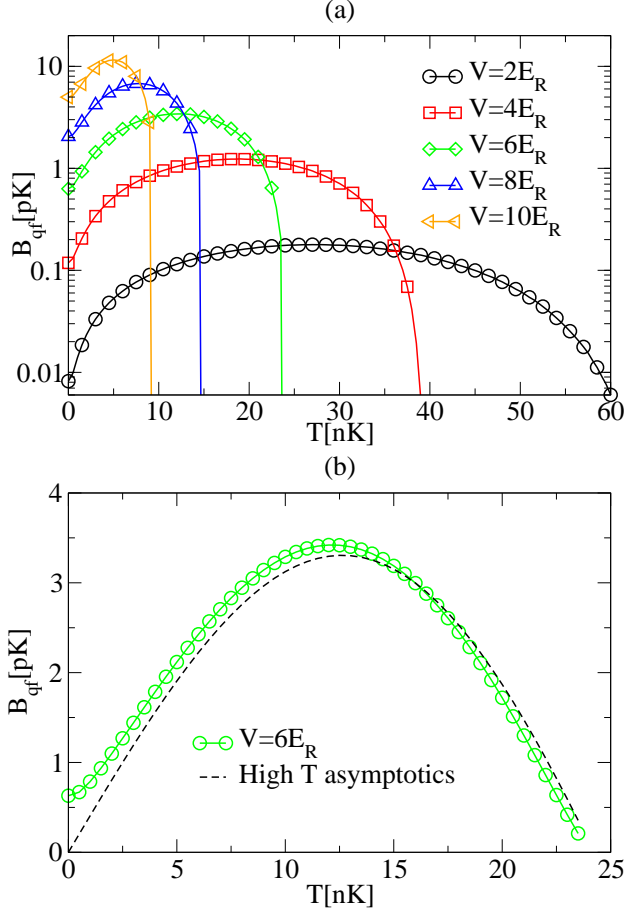


FIG. 10: (Color online) Induced free energy barrier height as a function of temperature for different lattice potentials. The dashed line in (b) is a plot for the high temperature asymptotics derived in Eq.(22). Note that thermal enhancement of barrier height is much less significant in deep optical lattices.

significant. At  $V = 10E_R$ , we find that the thermal effect only increases the potential by a few tens of percent and the potential can be predominately due to quantum fluctuations.

## V. EFFECTS OF SPIN EXCHANGE LOSSES

For  $F = 2$  rubidium atoms, the life time is mainly due to spin exchange losses that take place at a relatively short time scale of about 200ms[10, 11]. Note that three-body recombination usually occurs at a much longer time scale and has little effect on the time evolution studied here. Spin exchange losses put a very serve constraint on possible observations of *full* coherent oscillations driven by quantum fluctuations at frequencies well below 5Hz. To overcome this difficulty, we suggest to apply a quadratic Zeeman coupling close to  $q_{c1}$  ( $q_{c2}$ ) and study time evolution of state  $|2,0\rangle$  or  $\frac{1}{\sqrt{2}}(|2,2\rangle + |2,-2\rangle)$ . Regions of dynamical stability

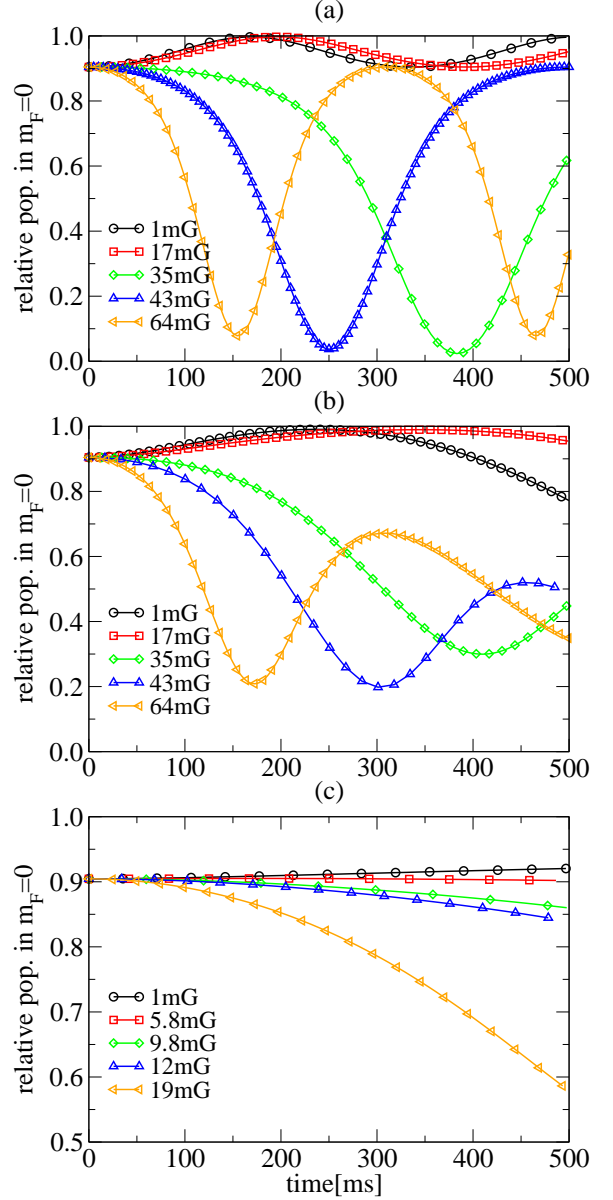


FIG. 11: (Color online) Estimated time evolution of rubidium population at  $|2,0\rangle$  hyperfine spin state when the quadratic Zeeman coupling or Zeeman field varies. (a) and (b) are for optical lattices with potential depth  $V = 10E_R$  and (c) is for  $V = 6E_R$ . In (a), we assume the density is uniform and there are no spin losses while (b) and (c) are for traps with inhomogeneous density and a finite loss rate  $1/\tau = (200ms)^{-1}$ . In (a),(b),(c), magnetic fields which yield dynamical critical quadratic Zeeman coupling  $q_{c1}$  ( $\sim q_{c2}$ ) are 35mG, 35mG and 10mG respectively.

of these states can be obtained by studying small oscillations around them as shown in section III. Results are summarized in Fig.9.

Dynamical stabilities of  $|2,0\rangle$  state below the threshold  $q_{c1}$ , or instabilities of  $(|2,2\rangle + |2,-2\rangle)/\sqrt{2}$  state

below threshold  $q_{c2}$  are directly induced by quantum fluctuations. Coherent quantum dynamics around state  $|2, 0\rangle$  ( $(|2, 2\rangle + |2, -2\rangle)/\sqrt{2}$ ) below and above dynamical critical coupling  $q_{c1}(q_{c2})$  are qualitatively different and it is therefore plausible to probe these dynamics that are driven mainly by quantum fluctuations at relative low frequencies. To explore this possibility, we have studied strongly damped population oscillations around a condensate  $|2, 0\rangle$  or a uniaxial state, at different quadratic Zeeman couplings when the spin exchange loss time is set to be 200ms. For this part of calculations we also take into account the density inhomogeneity of rubidium atoms in traps. Main results are shown in Fig.11 for different magnetic fields; at a given field, the corresponding quadratic Zeeman coupling is given as  $q_B = 3(\mu_B B/2)^2/6.8GHz$ .

Our major findings are three-folded and outlined below. Firstly, for a condensate with small deviations from  $|2, 0\rangle$  state, because of fast spin exchange losses complete coherent oscillations around  $|2, 0\rangle$  are hard to observe. Secondly, dynamics can be dramatically modified by a finite quadratic Zeeman coupling. When the coupling is much less than  $q_{c1}$  (defined for the density at the center of a trap), dynamics become slower when the quadratic Zeeman coupling increases. Beyond  $q_{c1}$ , dynamics become faster while the quadratic Zeeman coupling increases. These behaviors are consistent with results for the case of uniform density shown in the previous section; there, the oscillation frequency becomes zero at a dynamical critical coupling.

Thirdly (and perhaps most importantly), the population of atoms at state  $|2, 0\rangle$  always *grows* initially at short time scales when the quadratic Zeeman coupling is zero or smaller than  $q_{c1}$ , as a direct consequence of dynamical stabilities of a  $|2, 0\rangle$ -condensate. By contrast, beyond  $q_{c1}$  the population of atoms at state  $|2, 0\rangle$  always *decreases* initially at short time scales as a result of dynamical instabilities in this limit. These two distinct short-time behaviors of population at state  $|2, 0\rangle$  are signatures of a transition from quantum-fluctuation driven dynamics to a mainly quadratic Zeeman coupling driven dynamics. In the presence of strong spin losses, observing these distinct short-time asymptotics is an effective way to probe many-body quantum fluctuations in condensates we have considered. At very large quadratic Zeeman coupling, we have found expected rapid oscillations corresponding to mean field coherent dynamics and we don't show those results here. Finally, we also estimate the time-dependence of population oscillations at finite temperatures using thermal-fluctuation induced potentials discussed in a previous section. Thermal fluctuations usually speed up the coherent dynamics around state  $|2, 0\rangle$  when the quadratic Zeeman coupling is sufficiently weak (smaller than  $q_{c1}$ ); on the other hand, they can also slow down coherent dynamics around state  $|2, 2\rangle + |2, -2\rangle$  when a quadratic Zeeman coupling larger than  $q_{c2}$  is present. These results are shown in Fig.12. In obtaining these results, we have extrapolated

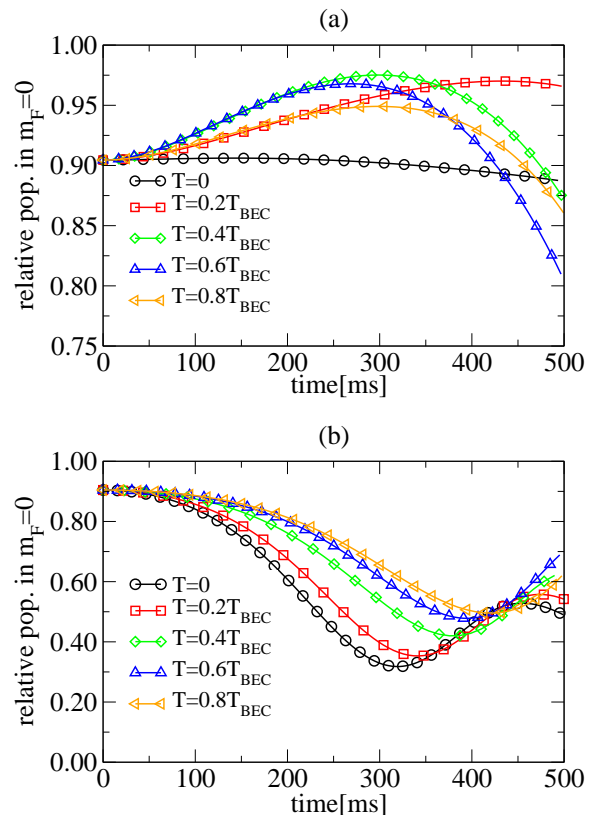


FIG. 12: (Color online) Estimated time evolution of population at  $|2, 0\rangle$  state at different temperatures. (a) is for a magnetic field of  $13mG$  that is below the dynamical critical field corresponding to  $q_{c1}$  and (b) is for  $38mG$  field which is above  $q_{c1}$ . The optical lattice potential depth is  $V = 8E_R$ ,  $T_{BEC} = 10.9nk$  and the spin exchange life time is again set to be  $200ms$ . Density inhomogeneity in traps has also been taken into account to obtain these plots.

the linear dynamical analysis into a regime where oscillation amplitude is substantial. So strictly speaking, results for  $35mG$ ,  $44mG$ ,  $65mG$  magnetic fields shown in Fig.11(b) are qualitative. However, short-time asymptotics that are the focuses of our discussions here are accurate.

## VI. CONCLUSION

In conclusion, we have demonstrated that unlike the usual mean-field-interaction driven coherent dynamics, *QFCS*D is a novel class of coherent dynamics fully driven by quantum fluctuations. These dynamics are conveniently tunable in optical lattices where oscillation frequencies can be varied by three to four order of magnitude. Frequencies of oscillations driven by quantum fluctuations have both distinct lattice-potential dependence and quadratic Zeeman-coupling dependence that can be studied experimentally. For rubidium atoms, *QFCS*D can be directly probed either at frequencies of a

few Hz or when the quadratic Zeeman coupling is about  $10^{-1}nk$ . One of potential applications of QFCS is perhaps the possibility of performing precise measurements of strongly correlated quantum fluctuations and critical exponents near quantum critical points. Current studies of critical correlations are based on analyzing statistics of interference fringes[36, 37]. Given the great control of coherent dynamics recently demonstrated for cold atoms[38], we would like to believe that quantum-fluctuation controlled dynamics might be an alternative and promising path towards probing critical correlations. Finally, we have also investigated the effects of finite temperatures, spin exchange losses and studied time evolution of condensates mainly driven by quantum fluctuations.

One of the authors(F.Z.) would like to thank KITP at Santa Barbara, Institute of Physics, Chinese Academy of Sciences, CASTU at TsingHua University in Beijing and Henry Poincare Institute in Paris for their hospitalities in the spring and summer of 2007. He also thanks Eugene Demler, Jason Ho, Wolfgang Ketterle, Gordon Semenoff and Klaus Sengstock for valuable discussions on experimental probing of QFCS. This work is supported by the office of the Dean of Science, University of British Columbia, NSERC(Canada), Canadian Institute for Advanced Research, and the Alfred P. Sloan foundation.

## APPENDIX A: COLLECTIVE COORDINATES

To study QFCS, we expand  $\psi^\dagger$  about a reference condensate  $\chi$ ,

$$\hat{\psi}_{k,\alpha\beta}^\dagger = \sqrt{4M}\chi_{\alpha\beta}(\xi) + \frac{1}{\sqrt{N_T}} \sum_{\nu} L_{\alpha\beta}^{\nu} (\hat{\theta}_{\nu}^\dagger(0) + \sum_{\mathbf{q}\neq 0} e^{i\mathbf{q}\cdot\mathbf{r}_k} \hat{\theta}_{\nu}^\dagger(\mathbf{q})) \quad (\text{A1})$$

Here  $N_T$  is the number of lattice sites and  $M$  is the number of atoms per site. The superscripts (or subscripts)  $\nu = x, y, z, \xi, p$  specify condensate motion along the five orthogonal directions of the submanifold.  $\hat{\theta}_{\nu}(\mathbf{q})$  ( $\hat{\theta}_{\nu}^\dagger(\mathbf{q})$ ) are annihilation (creation) operators of the collective excitations of mode  $\nu$  with lattice crystal momentum  $\mathbf{q}$ . One can further include bilinear terms in the expansion (not shown here). The motion along these five orthogonal directions is studied by introducing five mutually orthogonal matrices  $L^\nu$ , i.e.  $\text{Tr}(L^\mu L^\nu) = 2\delta_{\mu\nu}$ . Explicit forms of these orthogonal matrices were introduced previously[32].

We are restricting ourselves to the dynamics of a condensate in a linear regime. By expanding the original Hamiltonian in Eq.(1) using the decomposition introduced in Eq.(A1), we obtain an effective Hamiltonian that is bilinear in terms of  $\theta^\dagger$  and  $\theta$ . It is convenient to introduce five collective Hermitian operators  $\hat{X}_\nu$  defined

in terms of  $\theta_\nu^\dagger(0)$ ,  $\theta_\nu(0)$  for  $\mathbf{q} = 0$  modes,

$$\begin{aligned} \hat{X}_p &= \frac{\theta_p^\dagger - \theta_p}{2i\sqrt{N}}, \hat{X}_t = \frac{\theta_t^\dagger + \theta_t}{2\sqrt{N}}, \\ \hat{X}_x &= \frac{\theta_x^\dagger + \theta_x}{4\sqrt{N}(\chi_{yy} - \chi_{zz})}, \\ \hat{X}_y &= \frac{\theta_y^\dagger + \theta_y}{4\sqrt{N}(\chi_{zz} - \chi_{xx})}, \\ \hat{X}_z &= \frac{\theta_z^\dagger + \theta_z}{4\sqrt{N}(\chi_{xx} - \chi_{yy})} \end{aligned} \quad (\text{A2})$$

where  $N = N_T M$  is the total number of atoms in a lattice with  $N_T$  sites. By comparing Eq.(A1) and the expression for  $\tilde{\chi}$  in terms of five spin coordinates  $X_\nu$  (see discussions before Eq.(8)), one identifies the semiclassical collective coordinates  $X_\nu$  as the expectation value of harmonic oscillator operators  $\hat{X}_\nu$ . In the following, we do not distinguish between  $\hat{X}_\nu$  and  $X_\nu$ . The conjugate momentum operators  $\hat{P}_\nu$  can be introduced accordingly so that the usual commutation relations are obeyed, i.e.  $[\hat{X}_\nu, \hat{P}_\mu] = i\delta_{\nu\mu}$ .

**Quantum-fluctuation-induced potentials** Five modes of zero point motions (microscopic) around  $\chi(\xi)$  can also be labelled by the same set of indices. For collective excitations of mode- $\nu$  with lattice momentum  $\mathbf{q} (\neq 0)$ , creation operators are  $\theta_\nu^\dagger(\mathbf{q})$ . These operators obey the bosonic commutation relations,  $[\theta_{k,\mu}, \theta_{l,\nu}^\dagger] = \delta_{kl}\delta_{\mu\nu}$ . Note that only the properties of three rotation modes and deformation mode ( $\xi$ -mode) depend on the value of  $\xi$ . The collective mode dispersion around  $\xi = 0$  or  $\xi = \pi/2$  has a very simple form,

$$E_{\nu,\mathbf{q}}(\xi, X_\xi, q_B) = \sqrt{\epsilon_{\nu,\mathbf{q}}[2m_{BN}v_\nu^2(\xi + X_\xi) + \epsilon_{\nu,\mathbf{q}}]}. \quad (\text{A3})$$

And in the expression for  $E_{\nu,\mathbf{q}}$ ,  $\epsilon_{\nu,\mathbf{q}} = 4t_L \sum_{\alpha} (1 - \cos q_{\alpha} d_L) + \kappa_{\nu} q_B$  is the energy of an atom with crystal quasi-momentum  $\mathbf{q} = (q_x, q_y, q_z)$ ;  $d_L$  is the lattice constant.  $m_{BN} = 1/(4t_L d_L^2)$  is the effective band mass.  $\kappa_{\nu}$ ,  $\nu = x, y, z, \xi$  are coefficients introduced in Eq.(12),(13).  $v_\nu$  is the sound velocity of the  $\nu$ -mode in the small- $|\mathbf{q}|$  limit,  $v_\alpha^2(\xi) = M(4b_L G_{\alpha\alpha} - c_L)/m_{BN}$ ,  $v_\xi^2 = M|c_L|/m_{BN}$ .  $G_{\alpha\beta}(\xi)$  is a function of  $\xi$  introduced in Eq.(13).

When the quadratic Zeeman coupling is zero, the energy dispersion was also derived in a previous work of ours[32]. The dispersion of the  $\xi$ -mode in this case is independent of  $\xi$  or  $X_\xi$ . And among four gapless spin modes, only the  $x$ -,  $y$ - and  $z$ - spin rotational modes contribute to the  $\xi$ -dependence of the quantum fluctuation-induced potential  $V_{qf}$ . Substituting Eq.(A3) into Eq.(12), one obtains the quantum-fluctuation-induced potential  $V_{qf}$ . In 3d optical lattices, we find that the  $\xi$ -dependent energy potential is proportional to  $\sum_{\alpha} v_{\alpha}^5/(d_L^5 t_L^4)$ ,  $d_L$  is the lattice constant and  $t_L$  is the hopping integral. In 2d lattices,

the  $\xi$ -dependent energy potential  $V_{qf}(\xi)$  is proportional to  $\sum_{\alpha} v_{\alpha}^4 / (d_L^4 t_L^3) \ln t_L d_L / v_{\alpha}$ . These calculations lead to the scaling behaviors discussed in Eq.(14). When the quadratic Zeeman coupling is present, we find that for  $\xi = 0$ ,  $\kappa_{x,y,z,\xi}$  are not positive defined and collective spin modes can be unstable. To calculate induced-potential  $V_{qf}$ , we include stable modes ( $\mathbf{q} \neq 0$ ) which contribute to the renormalization of adiabatic condensate dynamics. At  $\xi = \pi/2$ , all collective modes are stable.

**Condensate depletion** To study the condensate depletion in the optical lattice, we start from the effective Hamiltonian. Five collective modes on top of a nematic state are described by the following:

$$\mathcal{H} = \sum_{\nu,q} E_{\nu,q} \left( \tilde{\theta}_{\nu,q}^{\dagger} \tilde{\theta}_{\nu,q} + \frac{1}{2} \right). \quad (\text{A4})$$

Here  $\tilde{\theta}_{\nu,q}^{\dagger}$  and  $\tilde{\theta}_{\nu,q}$  are bosonic creation and annihilation operators for the  $\nu$ -th mode. These operators can be obtained by Bogoliubov transformations:

$$\tilde{\theta}_{\nu,q} = u_{\nu,q} \theta_{\nu,q} + v_{\nu,q} \theta_{\nu,-q}^{\dagger}, \quad (\text{A5})$$

$$\tilde{\theta}_{\nu,q}^{\dagger} = u_{\nu,q}^* \theta_{\nu,q}^{\dagger} + v_{\nu,q}^* \theta_{\nu,-q}. \quad (\text{A6})$$

The coefficients  $u_{\nu,q}$  and  $v_{\nu,q}$  are given:

$$u_{\nu,q} = \frac{1}{\sqrt{2}} \left( \sqrt{1 + \frac{m_{BN} v_{\nu,q}^2}{E_{\nu,q}}} + 1 \right)^{1/2}, \quad (\text{A7})$$

$$v_{\nu,q} = \frac{1}{\sqrt{2}} \left( \sqrt{1 + \frac{m_{BN} v_{\nu,q}^2}{E_{\nu,q}}} - 1 \right)^{1/2}. \quad (\text{A8})$$

Condensate deletions from the  $\nu$ -th mode with crystal momentum  $\mathbf{q}$  are

$$\langle \theta_{\nu,q}^{\dagger} \theta_{\nu,q} \rangle = (u_{\nu,q}^2 + v_{\nu,q}^2) \langle \tilde{\theta}_{\nu,q}^{\dagger} \tilde{\theta}_{\nu,q} \rangle + v_{\nu,q}^2. \quad (\text{A9})$$

Here  $\langle \tilde{\theta}_{\nu,q}^{\dagger} \tilde{\theta}_{\nu,q} \rangle$  is the occupation number of the  $\nu$ th mode and it is given by the Bose-Einstein statistics:

$$\langle \tilde{\theta}_{\nu,q}^{\dagger} \tilde{\theta}_{\nu,q} \rangle = \frac{1}{\exp(E_{\nu,q}/kT) - 1}. \quad (\text{A10})$$

Putting all these together, we reach the final equation to determine the condensate density:

$$M - M_0(T) = \frac{1}{N_T} \sum_{\nu,q \neq 0} \left( v_{\nu,q}^2 + \frac{u_{\nu,q}^2}{e^{\frac{E_{\nu,q}}{kT}} - 1} \right). \quad (\text{A11})$$

$M$  is the atom number density or number of atoms per lattice site and  $M_0$  is the condensed number density. The first term in the summation gives quantum depletion number due to the two body scattering and the second term gives the thermal depletion number. We solve the above equation numerically and the results are shown in Fig.1.

At zero temperature, quantum depletion is given by the term  $v_{\nu,q}^2$  which captures the effect of interactions or two body scattering processes. Our estimate shows that

$$\begin{aligned} 1 - \frac{M_0}{M} &\sim \sum_{\nu=p,\xi,x,y,z} \frac{1}{M} \left( \frac{m_{BN} v_{\nu}}{t_L d_L} \right)^3 \\ &\sim \frac{1}{M} \left( \frac{M a_L}{t_L} \right)^{3/2}. \end{aligned} \quad (\text{A12})$$

We have noticed that major contributions are from the phase fluctuations since  $a_L \gg |b_L|, |c_L|$ . In optical lattices when the potential depth  $V$  increases, the bandwidth  $t_L$  decreases exponentially as a function of  $V$  and  $a_L$  increases; as a result, quantum depletion grows as  $(\frac{a_L}{t_L})^{3/2}$ .

At finite temperatures,  $M_0$  decreases as temperature  $T$  increases and becomes zero at the transition temperature  $T_{BEC}$ . In the weakly interacting limit ( $t_L \gg a_L, b_L, |c_L|$ ), the condensate fraction is approximately equal to

$$\frac{M_0(T)}{M_0(T=0)} = 1 - \left( \frac{T}{T_{BEC}} \right)^{\frac{3}{2}}, \quad (\text{A13})$$

and  $T_{BEC} \sim 5M_0^{2/3} t_L$  in optical lattices.

- 
- [1] P. W. Anderson, *Basic Notations of Condensed Matter Physics* (Benjamin-Cummings, Menlo Park, 1984).  
[2] A. O. Caldeira and A. J. Leggett, *Ann. Phys.* **149**, 374 (1983).  
[3] I. Bloch, T. W. Hänsch, and T. Esslinger, *Phys. Rev. Lett.* **82**, 3008 (1999).  
[4] M.-O. Mewes, M. R. Andrews, D. M. Kurn, D. S. Durfee, C. G. Townsend, and W. Ketterle, *Phys. Rev. Lett.* **78**, 582 (1997).  
[5] D. S. Hall, M. R. Matthews, C. E. Wieman, and E. A. Cornell, *Phys. Rev. Lett.* **81**, 1543 (1998).  
[6] B. P. Anderson and M. A. Kasevich, *Science* **282**, 1686 (1998).  
[7] J. R. Abo-Shaeer, C. Raman, J. M. Vogels, and W. Ketterle, *Science* **292**, 476 (2001).  
[8] J. Stenger, S. Inouye, D. M. Stamper-Kurn, H.-J. Miesner, A. P. Chikkatur, and W. Ketterle, *Nature* **396**, 345 (1998).  
[9] H.-J. Miesner, D. M. Stamper-Kurn, J. Stenger, S. Inouye, A. P. Chikkatur, and W. Ketterle, *Phys. Rev. Lett.* **82**, 2228 (1999).  
[10] H. Schmaljohann, M. Erhard, J. Kronjäger, M. Kottke, S. van Staa, L. Cacciapuoti, J. J. Arlt, K. Bongs, and K. Sengstock, *Phys. Rev. Lett.* **92**, 040402 (2004).

- [11] M. S. Chang, Q. S. Qin, W. X. Zhang, L. You, and M. S. Chapman, *Nature Phys.* **1**, 111 (2005).
- [12] J. M. Higbie, L. E. Sadler, S. Inouye, A. P. Chikkatur, S. R. Leslie, K. L. Moore, V. Savalli, and D. M. Stamper-Kurn, *Phys. Rev. Lett.* **95**, 050401 (2005).
- [13] T.-L. Ho, *Phys. Rev. Lett.* **81**, 742 (1998); C. V. Ciobanu, S.-K. Yip, and T.-L. Ho, *Phys. Rev. A* **61**, 033607 (2000).
- [14] T. Ohmi and K. Machida, *J. Phys. Soc. Jpn.* **67**, 1822(1998).
- [15] S. Coleman and E. Weinberg, *Phys. Rev. D* **7**, 1888 (1974).
- [16] E. F. Shender, *Sov. Phys. JETP* **56**, 178 (1982).
- [17] C. L. Henley, *Phys. Rev. Lett.* **62**, 2056 (1989).
- [18] D. Jaksch, C. Bruder, J. I. Cirac, C. W. Gardiner, and P. Zoller, *Phys. Rev. Lett.* **81**, 3108 (1998).
- [19] M. Greiner, O. Mandel, T. Esslinger, T. W. Hänsch, and I. Bloch, *Nature* **415**, 39(2002).
- [20] S. Fölling, F. Gerbier, A. Widera, O. Mandel, T. Gericke, and I. Bloch, *Nature* **434**, 481 (2005).
- [21] G. K. Campbell, J. Mun, M. Boyd, P. Medley, A. E. Leanhardt, L. G. Marcassa, D. E. Pritchard, and W. Ketterle, *Science* **313**, 649 (2006).
- [22] T. Stöferle, H. Moritz, C. Schori, M. Köhl, and T. Esslinger, *Phys. Rev. Lett.* **92**, 130403 (2004).
- [23] C. C. Tsai, R. S. Freeland, J. M. Vogels, H. M. J. M. Boesten, B. J. Verhaar, and D. J. Heinzen, *Phys. Rev. Lett.* **79**, 1245 (1997).
- [24] Ph. Courteille, R. S. Freeland, D. J. Heinzen, F. A. van Abeelen, and B. J. Verhaar, *Phys. Rev. Lett.* **81**, 69 (1998).
- [25] R. Wynar, R. S. Freeland, D. J. Han, C. Ryu, and D. J. Heinzen, *Science* **287**, 1016 (2000).
- [26] E. G. M. van Kempen, S. J. J. M. F. Kokkelmans, D. J. Heinzen, and B. J. Verhaar, *Phys. Rev. Lett.* **88**, 093201 (2002).
- [27] J. L. Roberts, N. R. Claussen, J. P. Burke, C. H. Greene, E. A. Cornell, and C. E. Wieman, *Phys. Rev. Lett.* **81**, 5109 (1998).
- [28] N. N. Klausen, J. L. Bohn, and C. H. Greene, *Phys. Rev. A* **64**, 053602 (2001).
- [29] A. Widera, F. Gerbier, S. Fölling, T. Gericke, O. Mandel, and I. Bloch, *Phys. Rev. Lett.* **95**, 190405 (2005).
- [30] F. Zhou and G. W. Semenoff, *Phys. Rev. Lett.* **97**, 180411 (2006).
- [31] G. W. Semenoff and F. Zhou, *Phys. Rev. Lett.* **98**, 100401(2007).
- [32] J. L. Song, G. W. Semenoff, and F. Zhou, *Phys. Rev. Lett.* **98**, 160408 (2007).
- [33] A. Turner, R. Barnett, E. Demler, and A. Vishwanath, *Phys. Rev. Lett.* **98**, 190404 (2007).
- [34] W. E. Lamb and R. C. Retherford, *Phys. Rev.* **72**, 241 (1947).
- [35] State  $|2, 0\rangle$  becomes unstable along the directions of  $X_{x,y}$  in the presence of a finite  $q_B$ . Coherent oscillations discussed here can be observed if initial states are prepared precisely. More robust oscillations are those around states that correspond to global potential minima shown in Fig.6b. See more discussions below.
- [36] A. Polkovnikov, E. Altman, and E. Demler, *Proc. Nat. Acad. Sci.* **103**, 6125 (2006).
- [37] Z. Hadzibabic, P. Krüger, M. Cheneau, B. Battelier, and J. Dalibard, *Nature* **441**, 1118 (2006).
- [38] J. M. Obrecht, R. J. Wild, M. Antezza, L. P. Pitaevskii, S. Stringari, and E. A. Cornell, *Phys. Rev. Lett.* **98**, 063201 (2007).